Journal of Power Sources 247 (2014) 307–313

Contents lists available at ScienceDirect

Journal of Power Sources

journal homepage: www.elsevier.com/locate/jpowsour

Short communication

A new approach to surface properties of solid electrolyte interphase on a graphite negative electrode

Seon-Hong Lee*, Ho-Gon You, Kyu-Suk Han, Jake Kim, In-Ho Jung, Joo-Han Song

Corporate R&D Center, Samsung SDI Co. Ltd., Yongin 446-577, Gyunggido, Republic of Korea

HIGHLIGHTS

- A new method for observing the outermost surface morphology and the thickness of SEI are presented.
- SEI layer surface becomes more differentiated SEM image under low acceleration voltage.
- Spongy-type SEI layer could be composed of the compact inner layer and the porous outer layer.

GRAPHICAL ABSTRACT

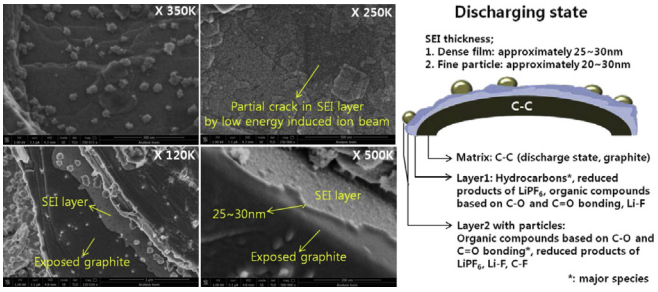

ARTICLE INFO

Article history:
Received 30 July 2013
Received in revised form
26 August 2013
Accepted 28 August 2013
Available online 4 September 2013

Keywords:
Lithium-ion battery
Graphite
Solid electrolyte interphase
Low acceleration voltage
Monte Carlo simulation
Ion etching

ABSTRACT

A new method for observing the outermost surface morphology and the thickness of solid electrolyte interphase (SEI) are presented. Low acceleration voltage in extreme high resolution scanning electron microscopy (XHR-SEM) provides detailed information on the SEI surface morphology due to secondary electron contrast mechanism. Also, XHR-SEM under low acceleration voltage with low energy induced ion etching in x-ray photoelectron spectroscopy (XPS) studies provides valuable information on the SEI layer thickness. More detailed properties of the SEI layer were investigated by transmission electron microscopy (TEM).

1. Introduction

Graphite-based negative electrodes are widely used in commercially available lithium-ion battery (LIB). During the initial intercalation of lithium into the graphite negative electrode, the intercalated lithium reacts immediately with the electrolyte, and forming a passive layer called solid electrolyte interphase (SEI) [1–3]. Many researchers have reported the role of SEI layer on various electrolytes (or cathode/anode material), and the various mechanisms have been proposed to account for the relation between SEI characterization and cell performance [4–11]. Reactions for various electrolyte components at graphite surfaces are described in Refs. [3–8,12–14]. Those processes continue until the electrode surface is completely covered and the SEI thickness exceeds at least the tunneling capability of electrons (a few nano size) [1]. The SEI properties influence on cell performance such as power capability, self discharge, performance at low/high temperature and safety [15] and therefore it is very important to

* Corresponding author. Tel.: +82 10 6488 0381; fax: +82 31 288 4447.
E-mail address: pookter@naver.com (S.-H. Lee).

0378-7753/$ – see front matter © 2013 Elsevier B.V. All rights reserved.
http://dx.doi.org/10.1016/j.jpowsour.2013.08.105

control the SEI film formation for the LIB industry. However, the formation mechanism and its composition of SEI caused by electrochemical reaction on the graphite electrode/electrolyte interface are not clearly understood and have been debated for a long time.

Meanwhile, many researchers have reported the morphological properties of SEI layer on anode material using SEM images. However, they did not consider the effect of acceleration voltage in SEM analysis for observing the SEI layer. In fact, at low beam voltage, the surface becomes more differentiated image due to secondary electron contrast mechanism which could represent more detailed surface chemistry. Surface techniques such as X-ray Photoelectron Spectroscopy (XPS), Auger electron Spectroscopy (AES) and Secondary ion mass spectroscopy (SIMS) have been used to measure the SEI layer thickness by depth profiling. However, it is difficult to obtain reasonable thickness data from those depth profiling techniques because of its rough and inhomogeneous morphology [16]. In fact, its thickness can vary from 15 to 900 Å on the same electrode [17]. Morphological studies such as Focused Ion Beam (FIB)–Transmission Electron Microscopy (TEM) [18] are also reported, but this technique has still unresolved questions; ion beam at high voltage (or current density) causes significant chemical damage [19–21]. The atomic force microscopy (AFM) [22–25] is also reported for estimating the SEI film thickness, but this technique needs to highly technical know-how for in-situ system, and does not shown the SEI (or graphite) components at the same sample location.

In the present study, we investigate a new approach to characterize the SEI surface properties on the graphite using extreme high resolution scanning electron microscopy (XHR-SEM) under low acceleration voltage, and to investigate the thickness measurement with low energy induced ion etching in XPS. Also, we investigate the cross-sectional FIB-milled microstructures with TEM and Electron Energy-loss Spectroscopy (EELS) which are used to observe the morphologies and components of the detailed SEI structures for comparison.

2. Experimental

The LIB cells were constructed using doped-LCO cathode active material and pitch coated natural graphite as the active anode material. The anode electrodes included carbon black for conductivity enhancement with styrene butadiene rubber (SBR) as the binder dissolved in anhydrous *N*-methyl-2-pyrrolidinone (NMP). The resulting slurry was cast on a copper foil. The composite electrode was then dried in a convection oven at 110 °C for 2 h. The cathode also included carbon black, 10% PVDF binder on 10 mm copper foil. The conventional organic electrolyte was 1 M LiPF6 dissolved in the mixtures of ethylene carbonate (EC), ethylmethyl carbonate (EMC), and diethyl carbonate (DEC) in a volume ratio of 3:5:2. As additives to the electrolyte solution, 1 wt.% vinylene carbonate (VC) and 3 wt.% fluoroethylene carbonate (FEC) were used. The water content in the electrolyte solutions was less than 10 ppm. A prismastic-type cell was assembled/disassembled in an argon-filled glove box (<1 ppm H_2O, <10 ppm O_2) to prevent from moisture/air exposure.

For the SEI formation the cell was charged to 4.2 V, and then discharged to 3.0 V at a rate of 0.5 C in one cycle using a constant current–constant voltage (CC–CV) protocol, and was disassembled in an argon-filled glove box.

Chemical bonding states and concentration of each element at the surface were analyzed by XPS (VG, ESCALAB250) using a monochromatic Al Ka radiation ($h\nu$ = 1486.6 eV). Each layer components for the sample surface by Ar^+ ion etching can provide useful information on the morphological features of the SEI surface. Ion energies about 300 eV with yielding ion currents of 1.0 μA were used to minimize surface damage [15,26]; the chemical bonding of organic materials is prone to severe sputter damage, which could make it difficult to interpret them with XPS using conventional conditions (Recently, Ar cluster and C_{60} ion guns have successfully been employed for non-destructive depth profiling of organic materials [27,28]). The etching rate with argon gun was roughly determined with a SiO_2 sample (approximately 2.5 nm min^{-1}) as a reference. Although this measured SEI thickness may not indicate the absolute value, this procedure may understand appropriate to compare relatively SEI thickness (In fact, during the destructive depth analysis of inhomogeneous films, the etching rate is not the same for hard and soft components. The hard inorganic materials (Li_2O, LiF, Li_2CO_3 etc.) need longer sputtering time to etch a particular depth as compared to the soft organic material). The ion gun geometry gave an incident angle of the $Ar^{\pm}$ ions of 45° to the sample surface. A flood gun source was used to compensate the charging effect. For high-resolution measurements of the target elements, constant pass energy was set to 24.5 eV. The spectrometer was calibrated using the photoemission line Ag $3d_{5/2}$ (binding energy 368.3 eV). For the Ag $3d_{5/2}$ line the full width at half maximum (FWHM) was 0.58 eV under the recording conditions. The analyzed area of the samples was 500 × 500 μm^2. The base pressure of the XPS system was less than 2 × 10^{-10} mbar and the working pressure was less than 8 × 10^{-9} mbar. The dimethyl carbonate (DMC) rinse (conducted in a glove box) was used to remove electrolyte salt residues during 15 min and then dried for 6 h in a glove box. For the deconvolution of the XPS spectra a mixed Gaussian–Lorenzian function in the Avantage software was used.

The morphological characterization of SEI layer surface was investigated with an XHR-SEM (FEI, Magellan 400) using various accelerating voltage of 1, 5 and 10 kV. The thickness for the SEI layer was estimated as following processes;

i) SEI bonding properties at the outermost surface and inner part layer (after ion etching for 2 min) were analyzed by XPS. To minimize the surface damage from high energy induced ion etching [21,26,29], the etching conditions were set as 1 kV and 0.2 μA.
ii) The holder take out from XPS pre-chamber under N_2 atmosphere and then move directly to an argon-filled glove box. The samples were taken off from XPS holder and then sampling again on transfer holder to XHR-SEM [30].
iii) Transfer holder take out from glove box, and insert to the load-lock chamber in XHR-SEM.

In order to compare the obtained results, the micro-structure and the local chemical compositions of the SEI layer were examined by TEM (FEI, Tecnai F30) equipped with Gatan image filter spectrometer (GIF-2000). TEM-EELS with high spatial resolution can provide valuable information on lithium spatial distribution and its chemical states in the SEI layer. However, light elements such as the lithium species were extremely susceptible to radiolysis damage and knock-on displacement during electron beam irradiation. For reducing these sputtering damages, TEM was operated at 300 kV. Recent TEM study on lithium intercalated graphite clearly demonstrated that this experimental condition may be very optimal for examining the SEI layer because sputtering cross-sections of carbon and lithium compounds exponentially decrease with the accelerating voltage [31]. Using FIB, the sample was thinned to a thickness of approximately 100 nm, and then transferred to the TEM within 2 min for minimizing air exposure.

3. Results and discussion

Fig. 1(a, b, c) shows the variation in beam interaction volume with energy by using a Monte Carlo simulation (CASINO ver. 2.42, the graphite density was set to 2.28 g cm^{-3}) [32] of the electron trajectories in the graphite surface. This result confirms that the conventional energies (10 kV, 5 kV) can observe the bulk of a graphite anode, approximately 320–1000 nm, while the low beam voltage (1 kV) can observe the outermost surface regions, approximately 20–25 nm. Therefore, the low voltage image can be more sensitive to the chemical nature and topographic form of the SEI layer on graphite due to its thickness range of a few nano size. This is demonstrated in Fig. 1(d, e, f) which shows secondary electron (SE) images of the SEI layer on the graphite anode for various accelerating voltage information cell. At the 10 kV (Fig. 1(d)), a typical SE image, the contrast effect is almost negligible compare with 5 kV (Fig. 1(e)) and 1 kV (Fig. 1(f)). At the 1 kV, the SEI layer surface becomes more differentiated image due to secondary electron contrast mechanism which represents more detailed information on the surface chemistry [33]. This is similar to other reported studies on semiconductors, which also report a maximum contrast effect for incident electron energy in the range 1–2 kV [34–36]. Therefore, this may provides new understanding of the SEI features. These results indicate that more detailed morphological analysis for the outermost surface of SEI layer is required to observe under low acceleration voltage (around 1 kV) in XHR-SEM. We have also tried to observe at below the 1 kV (not shown here) but the SEM image of the SEI layer has shown noticeable distortion during observation due to the surface contamination charging from adsorbed hydrocarbons [37], and the resolution image becomes lower.

The schematic illustration of the principle for SEI thickness observation is shown in Fig. 2. The incident angle for the argon ion beams was 45° from the anode electrode surface, as shown in Fig. 2(a). When the incident beam strikes the anode surface, all graphite particles are exposed to the etching yield, but only the shadow area by the around graphite particles is not exposed, as shown in Fig. 2(b). After a proper etching time the SEI layer exposed to the etching yields is almost removed and then exposes the graphite surface. The thickness of SEI layer could be observed at the step area between exposed etching yields and does not exposed etching yields.

Fig. 3 shows the outermost surface and cross-sectional secondary electron SEM images for the graphite anode electrode with before (Fig. 3(a)) and after (Fig. 3(b–d)) inducing low energy ion etching in XPS. The etching time of the samples were set to 2 min (Fig. 3(b)) and 5 min (Fig. 3(c, d, e)). The SEI layer shows the existence of fine particles (approximately 20–30 nm) on the dense surface film, as shown in Fig. 3(a). After an ion etching time for 2 min, the dense film surface shows partial crack by ion beam, as shown in Fig. 2(b). After 5 min, the SEI layer in the ion beam exposed area is almost removed and then exhibit the exposed graphite surface, as shown in Fig. 3(c, d, e). However, after ion etching for 5 min the traces of most particles are still remain onto graphite (and/or film layer), and the graphite grain boundaries are clearly observed, as shown in Fig. 3(e), suggesting that most layer film could be removed but the particles does not removed all, probably due to the thickness difference between film part and particle part. The thickness of the SEI layer at the step area between exposed area and shadow area was roughly estimated to be 25–30 nm, as shown in Fig. 3(d), where the roughly thickness and topology of the SEI layer are similar to those reported by Jeong et al. [25].

In order to analyze chemical bonding states (and concentration of each element) near the film surface, two XPS narrow-scan spectra (C1s and F1s) of the outermost part for the SEI layer was obtained in Fig. 4(a), and then Ar^{+} etching for 2 min was performed to investigate the inner part of the SEI layer in Fig. 4(b) (Li 1s and O 1s peak spectra are not shown here due to their poor information because most lithium/oxygen-containing species (Li_2O, Li_2CO_3, LiOH etc.) present very few variations (broad peaks) in binding energy). The C 1s spectra were fitted with four peaks according to

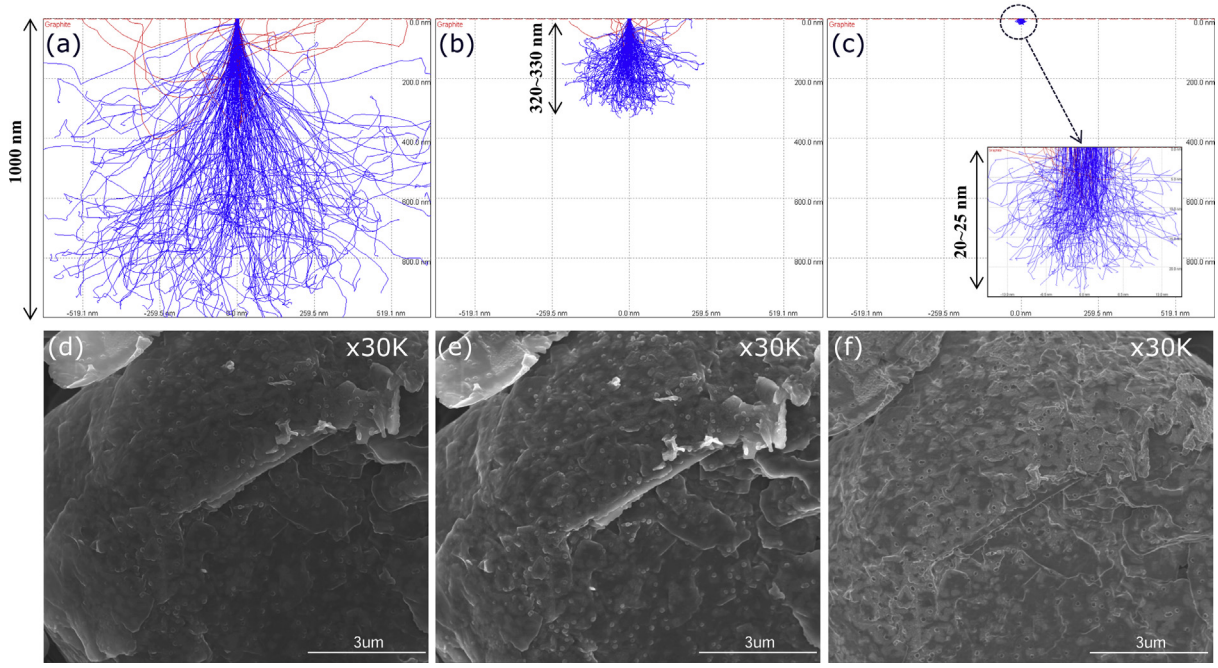

Fig. 1. Interaction volume of electrons in graphite at (a) 10, (b) 5 and (c) 1 kV beam energies using Monte Carlo simulation (the primary electrons are shown in blue, with backscattered electrons in red), and SEM images of SEI surface on graphite anode information cell under an accelerating voltage at (d) 10, (e) 5 and (f) 1 kV. (For interpretation of the references to color in this figure legend, the reader is referred to the web version of this article.)

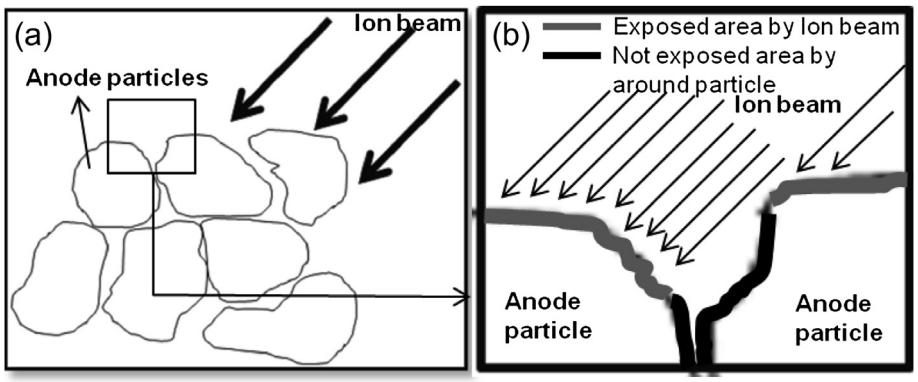

Fig. 2. The schematic illustration of the principle for SEI thickness observation by ion beam etching in XPS.

the reported binding energies; C–F or CO_3-like at 291 eV, O–C=O at 288.5 eV, C–O at 286.5 eV, and C–H at 285 eV [14,16,38,39]. The F 1s spectra are fitted with three peaks centered at 689 eV (C–F), 687–688 eV (reduction products of $LiPF_6$) and 685.5 eV (Li–F) [13–16,38,39]. It is noted that the outermost surface of the SEI layer shows quite different features compared with the inner part of those SEI layers, implying difference of SEI chemical bonding state. The details of the fitted results on the surface species and peak area (atomic concentration, at.%) of both samples are showed in Fig. 5. The hydrocarbon (C–H), Li–F and reduction products of $LiPF_6$ bonding concentrations at the outermost surface increase after ion etching for 2 min, while the C–O, O–C=O, $-CO_3$ and C–F bonding

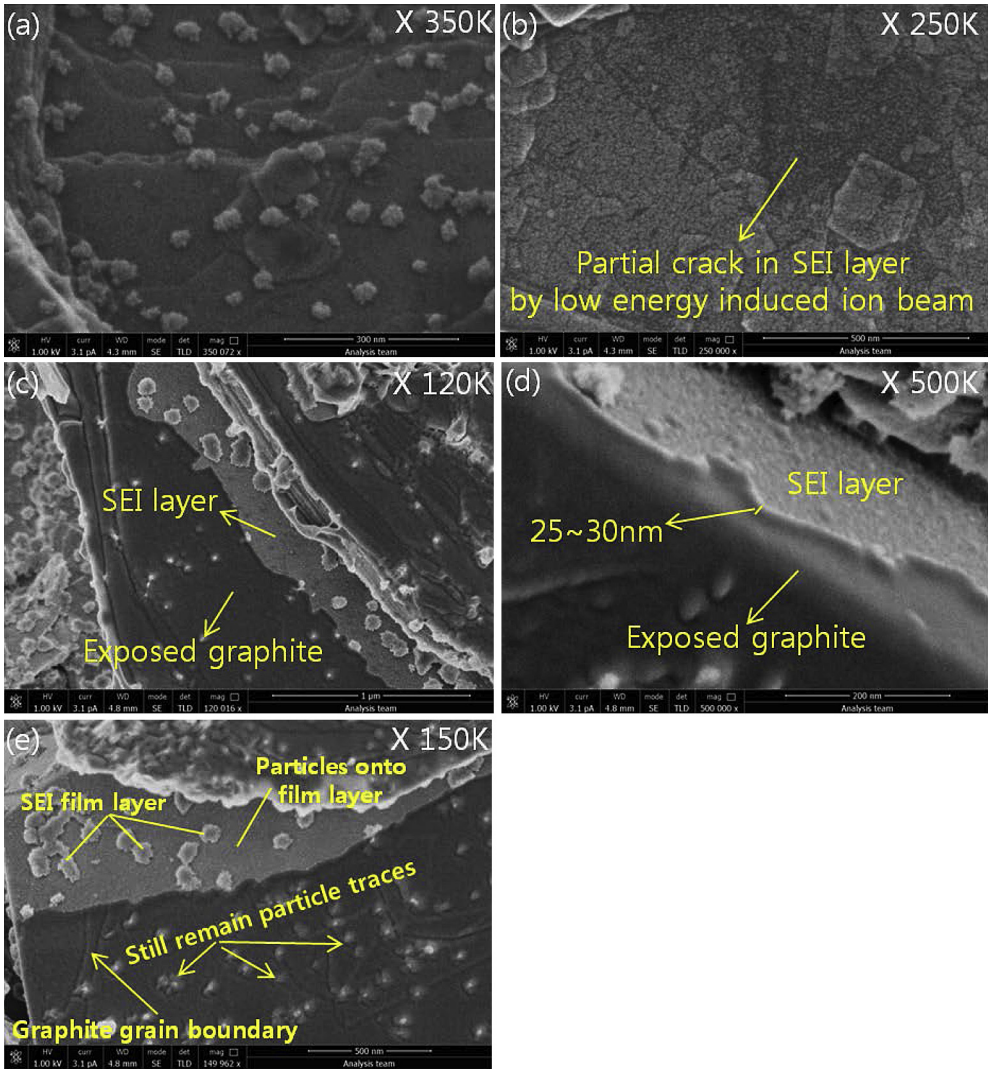

Fig. 3. XHR-SEM images of SEI layer on graphite electrode for formation cell: (a) before ion etching (b) after ion etching for 2 min and (c, d, e) after ion etching for 5 min.

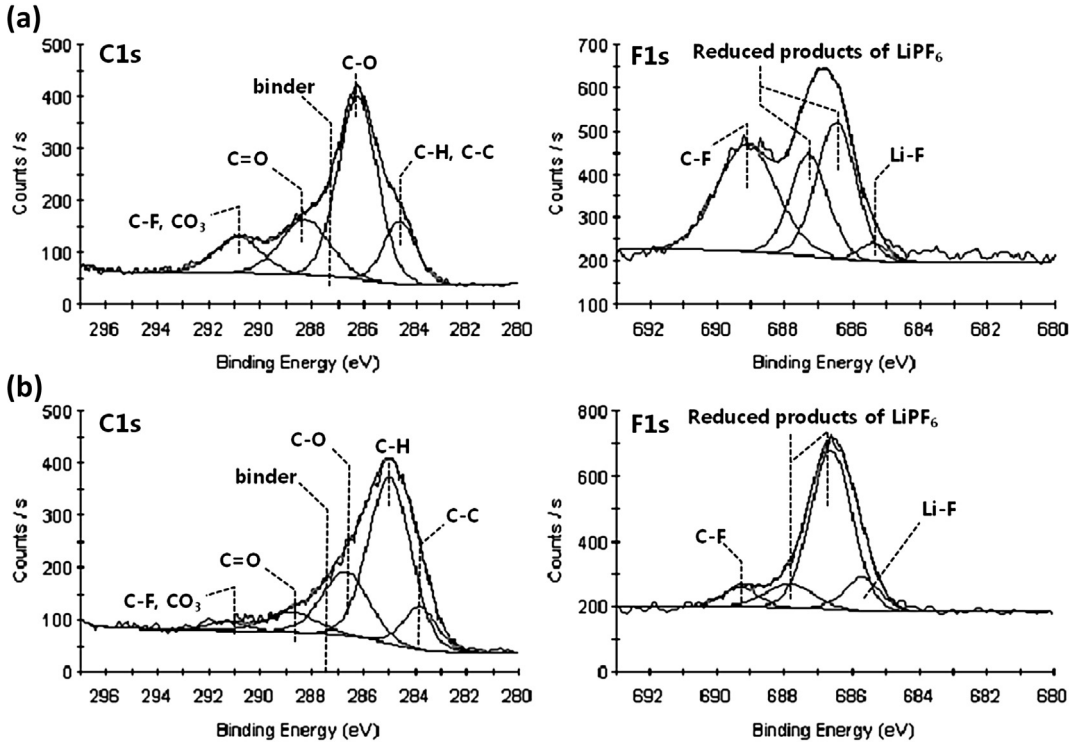

Fig. 4. XPS deconvoluted C 1s and F1s spectra for anode electrode information cell; (a) before ion etching (b) after ion etching for 2 min.

concentration decreases. Among them, the hydrocarbon, C—O and reduction products of $LiPF_6$ are major component of the whole SEI layer. The organic C—O and C═O peaks are larger in the film derived from the VC-added electrolyte [40,41], while the hydrocarbon (C—H) peak around 285 eV has been assigned to oxygen-containing chain like polyethylene oxide (PEO)-type polymer from polymerization of EC in the SEI layer [16,40]. Therefore, it is suggested that the outermost layer of the SEI is mainly composed of the polymer species from the VC-additive, and the inner layer of the SEI is mainly composed of the polymer species from the EC. These results may explain the reduction behavior in the cyclic voltammetry measurements [40]. The reduction products of $LiPF_6$ are main composition of inorganic species for both outermost layer and inner parts layer, while the Li—F bonding exhibit slight (the C—F bonding may originates from decomposed PVDF binder in the cathode and the degradation productions could be transported to the SEI layer surface on graphite anode). It is likely that solvent molecules from $LiPF_6$ could permeate into porous polymer layer by mainly EC and/or VC on the graphite surface, and therefore be reduced during formation process [16].

Fig. 6(a) shows a bright field TEM image of adjacent region shown in Fig. 3(a) where the interface between graphite and SEI is marked. The secondary particles are clearly observed at the surface where the morphology shows quite microscopically rough. Enlarged images of the secondary particles are shown in Fig. 6(b, c) with uncertain layer below. It is noted that the SEI layer of formation cell is consist of two type layer, i.e. the secondary particles layer with the thickness roughly within a range of 30—40 nm and the complex spongy-type layer with the thickness roughly within a range of 35—40 nm onto the graphite, corresponding to the XHR-SEM results in Fig. 3(d). The main component of the secondary particle appears to be LiF (and/or reduced $LiPF_6$ products), based on

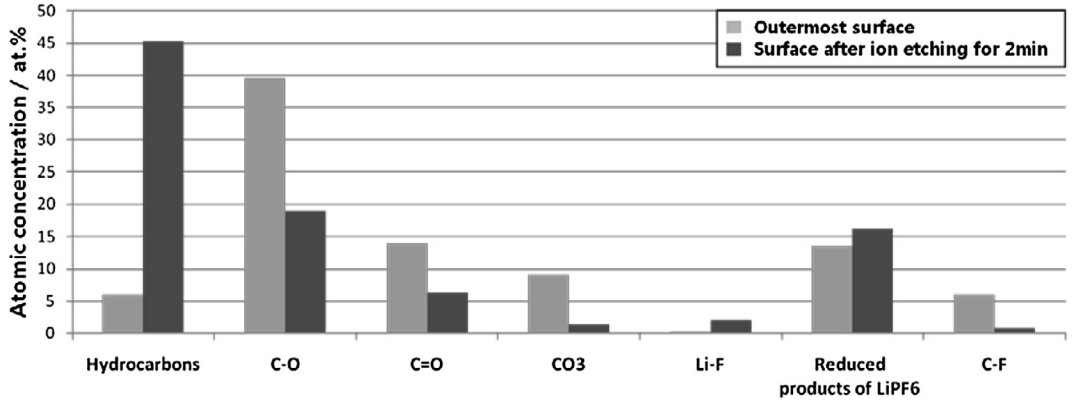

Fig. 5. Quantitative diagram of the surface species from XPS deconvoluted spectra for the anode electrode information cell; (dark black) outermost surface (gray) surface after ion etching for 2 min.

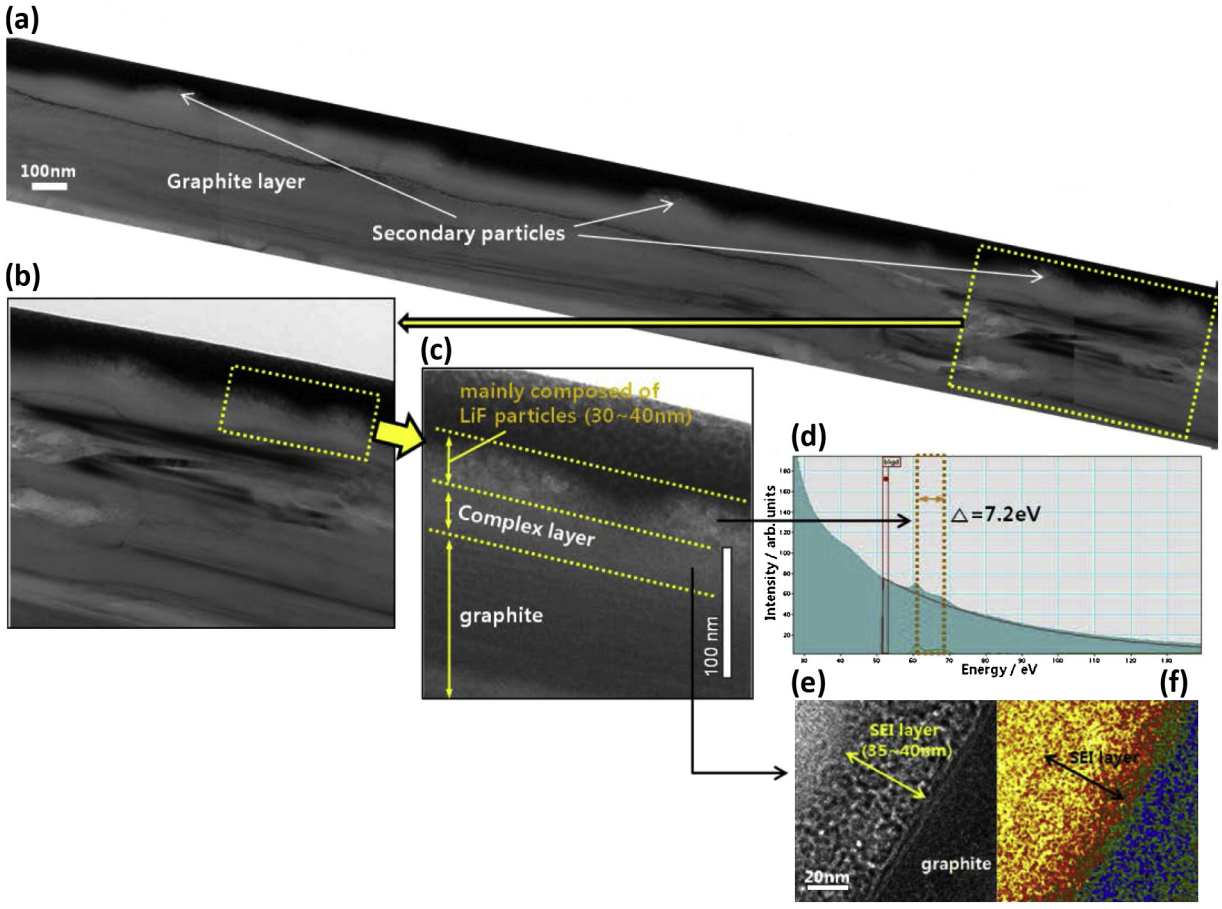

Fig. 6. (a) High-magnification bright-field TEM image of adjacent region shown in Fig. 3(a) at the SEI/graphite interface. (b) Enlarged image [marked as (b) in (a)]. (c) Enlarged image [marked as (c) in (b)]. (d) EELS L1s spectra of the secondary particle. (e, f) HR-TEM image and EELS Li mapping of the region [shown as "complex layer" in (c)].

the shape of the Li K-edge spectra (energy gap exhibits 7.2 eV) in Fig. 6(d) [31]. These result consistent with the investigation by A. M. Andersson et al. [16]. The role of the secondary particles as SEI layer will be discussed in a latter paper. Fig. 6(e) clearly shows the spongy-type layer (like dense film) onto the graphite but the Li gradient of the layer (Fig. 6(f)) exhibit a non-uniform distribution, suggesting that the spongy-type layer could be composed of the compact inner layer (10–15 nm) and the porous outer layer (20–30 nm). It is likely that the spongy-type layer of the SEI may comprise the organic and/or inorganic components of the complex compact/porous structures. This complex feature requires further work on qualitative/quantitative analysis of the EELS spectra.

According to the XPS, XHR-SEM and TEM results, we proposed a schematic model for the SEI layer formed on graphite information cell, as shown in Fig. 7. The outermost layer (layer 2 with particles) of SEI is mainly composed of the polymer species (from VC) with reduction products of $LiPF_6$, and the inner layer (layer 1 onto graphite) of SEI is mainly composed of the polymer species (from EC) with reduction products of $LiPF_6$. The secondary particles (in layer 2) with the thickness roughly within a range of 20–30 nm and the complex spongy-type layer (dense film, layer 1) with the thickness roughly within a range of 25–30 nm onto the graphite are formed, and show inhomogeneous layer structure.

4. Conclusion

We have developed a new technique for measuring the thickness of SEI layer on graphite anode, and the surface morphological properties under low acceleration voltage was investigated by XHR-SEM. At the 1 kV, the SEI layer surface becomes more differentiated image which may provides new understanding of the SEI features. It is suggested that XHR-SEM under low acceleration voltage with low energy induced ion etching in XPS studies have provided valuable information on SEI layer formation. The outermost surface of the SEI layer shows quite different features compared with the

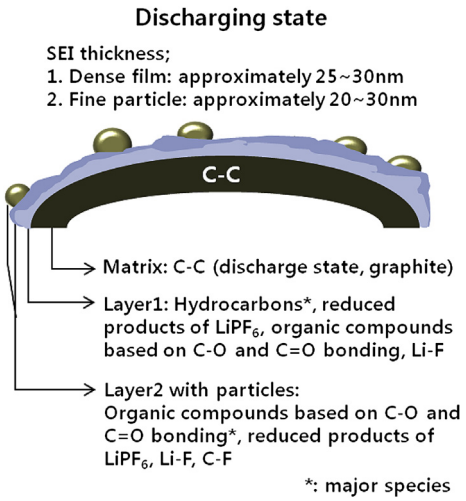

Fig. 7. Proposed model the SEI layer formed on graphite information cell.

inner part of those SEI layers. The spongy-type layer could be composed of the compact inner layer (10–15 nm) and the porous outer layer (20–30 nm).

References

[1] E. Peled, J. Electrochem. Soc. 126 (1979) 2047.
[2] R. Fong, U.V. Sacken, J.R. Dahn, J. Electrochem. Soc. 137 (1990) 2009.
[3] J.O. Besenhard, M. Winter, J. Yang, W. Biberacher, J. Power Sources 54 (1995) 228.
[4] D. Aurbach, M.L. Daroux, P.W. Faguy, E. Yeager, J. Electrochem. Soc. 134 (7) (1987) 1611.
[5] D. Aurbach, Y.E. Eli, B. Markovsky, A. Zaban, S. Luski, Y. Carmeli, H. Yamin, J. Electrochem. Soc. 142 (9) (1995) 2882.
[6] C. Wang, H. Nakamura, H. Komatsu, H.M. Yoshio, H.J. Yoshitake, J. Power Sources 74 (1998) 142.
[7] D. Aurbach, K. Gamolsky, B. Markovsky, Y. Gofer, M. Schmidt, U. Heider, J. Electrochem. Acta 47 (2002) 1423.
[8] K. Abe, H. Yoshitake, T. Kitakura, T. Hattori, H. Wang, M. Yoshio, J. Electrochem. Acta 49 (26) (2004) 4613.
[9] A.M. Andersson, D.P. Abraham, R. Haasch, S. MacLaren, J. Liu, K. Amine, J. Electrochem. Soc. 149 (2002) 1358.
[10] K. Abe, T. Takaya, H. Yoshitake, Y. Ushigoe, M. Yoshio, H. Wang, J. Electrochem. Solid-State Lett. 7 (2004) 462.
[11] Q. Zhang, H. Noguchi, H. Wang, M. Yoshio, M. Otsuki, T. Ogino, J. Chem. Lett. 34 (2005) 1012.
[12] D. Aurbach, B. Markovsky, I. Weissman, E. Levi, Y. Ein-Eli, Electrochim. Acta 45 (1999) 67.
[13] S. Leroy, H. Martinez, R. Dedryvere, D. Lemordant, D. Gonbeau, J. Appl. Surf. Sci. 253 (2007) 4895.
[14] P. Verma, P. Maire, P. Novak, J. Electrochem. Acta 55 (2010) 6332.
[15] A.M. Andersson, A. Henningson, H. Siegbahn, U. Jansson, K. Edström, J. Power Sources 522 (2003) 119.
[16] A.M. Andersson, K. Edström, J. Electrochem. Soc. 148 (2001) 1100.
[17] A.M. Andersson, Surface Phenomena in Li-ion Battery, Acta Universitatis Upsaliensis, Uppsala, 2001.
[18] S. Bhattacharya, A.R. Riahi, A.T. Alpas, J. Power Sources 196 (2011) 8719.
[19] J. Mayer, L.A. Giannuzzi, T. Kamino, J. Michael, J. Mater. Res. Soc. 32 (2007) 400.
[20] L.A. Giannuzzi, F.A. Stevie, Micron 30 (1999) 197.
[21] I.P. Jain, G. Agarwal, J. Surf. Sci. Rep. 66 (2011) 77.
[22] A.C. Chu, J.Y. Josefowicz, G.C. Farrington, J. Electrochem. Soc. 144 (1997) 12.
[23] K.A. Hirasawa, T. Sato, H. Asahina, S. Yamaguchi, S. Mori, J. Electrochem. Soc. 144 (1997) 4.
[24] S.K. Jeong, M. Inaba, T. Abe, Z. Ogumi, J. Electrochem. Soc. 148 (2001) 989.
[25] S.K. Jeong, M. Inaba, Y. Iriyama, T. Abe, Z. Ogumi, J. Power Sources 175 (2008) 540.
[26] E. Lewin, M. Gorgoi, F. Schafers, S. Svensson, U. Jansson, J. Surf. Coat. Technol. 204 (2009) 455.
[27] R. Hill, P. Blenkinsopp, A. Barber, C. Everest, J. Appl. Surf. Sci. 252 (2006) 7304.
[28] T. Miyayama, N. Sanada, S.R. Bryan, J.S. Hammond, M. Suzuki, J. Surf. Interface Anal. 42 (2010) 1453.
[29] A.M. Andersson, A. Henningson, H. Siegbahn, U. Jansson, K. Edström, J. Power Sources 119 (2003) 522.
[30] L.Y. Roussel, D.J. Stokes, I. Gestmann, M. Darus, R.J. Young, Proc. SPIE 7378 (2009), 73780W-1.
[31] F. Wang, J. Graetz, M.S. Moreno, C. Ma, L. Wu, V. Volkov, Y. Zhu, ACS Nano 5 (2011) 1190.
[32] D. Drouin, A.R. Couture, D. Joly, X. Tastet, V. Aimez, R. Gauvin, Scanning 29 (2007) 92.
[33] D.C. Joy, C.S. Joy, Micron 27 (1996) 247.
[34] D.D. Perovic, M.R. Castell, A. Howie, C. Lavoie, T. Tiedje, J.S.W. Cole, Ultramicroscopy 58 (1995) 104.
[35] C.P. Sealy, M.R. Castell, P.R. Wilshaw, J. Electron. Microsc. 49 (2000) 311.
[36] M. El-Gomati, F. Zaggout, H. Jayacody, S. Tear, K. Wilson, J. Surf. Interface Anal. 37 (2005) 901.
[37] A.E. Vladár, M.T. Postek, Proc. Microsc. Microanal. 11 (2) (2005) 764–765CD.
[38] J. Świątowska, V. Lair, C. Pereira-Nabais, G. Cote, P. Marcus, A. Chagnes, J. Appl. Surf. Sci. 257 (2011) 9110.
[39] L.E. Ouatani, R. Dedryvère, J.B. Ledeuil, C. Siret, P. Biensan, J. Desbrières, D. Gonbeau, J. Power Sources 189 (2009) 72.
[40] H. Ota, Y. Sakata, A. Inoue, S. Yamaguchi, J. Electrochem. Soc. 151 (2004) 1659.
[41] S.J. Park, J.H. Ryu, S.M. Oh, J. Electrochem. Soc. 158 (2011) 498.